Soft Matter

COMMUNICATION

View Article Online
View Journal | View Issue

Cite this: *Soft Matter*, 2016, **12**, 7726

Received 17th June 2016,
Accepted 30th August 2016

DOI: 10.1039/c6sm01381c

www.rsc.org/softmatter

Creasing of an everted elastomer tube†

Xudong Liang, Feiyu Tao and Shengqiang Cai*

A cylindrical elastomer tube can stay in an everted state without any external forces. If the thickness of the tube is small, the everted tube, except for the regions close to the free ends of the tube, maintains a cylindrical shape, and if the thickness is larger than a critical value, the cross-section of the everted tube becomes non-circular, which is caused by mechanical instability. Although eversion-induced instability in an elastomer tube has been reported several decades ago, a satisfying explanation of the phenomenon is still unavailable. In all previous studies, linear analyses have been adopted to predict the critical thickness of the tube for eversion-induced instability. The discrepancy between prediction and experiment is significant. In this communication, based on experiments and theoretical analyses, we show that crease formation on the inner surface of an everted tube is the mechanical instability mode, which cannot be captured by linear stability analyses. Instead, a combination of energetic analyses and numerical simulations of finite deformation in an everted tube enables us to correctly predict both the critical tube thickness for the onset of creases and the profile of the noncircular cross-section of an everted tube.

Turning a structure inside out, often called eversion, is ubiquitous in nature and frequently used in different fabrication processes. For example, during the development of the *Volvox* embryo, a spherical monolayer cell sheet turns itself inside out to achieve its adult configuration;[1] the eversion of jellyfish, known as 'Jellyfish syndrome', is a mechanism to protect itself from environmental changes;[2,3] and stent eversion has been used to construct an autologous heart valve, which is known as stent-biovalve.[4] Due to its profound influence in nature and in various engineering applications, the eversion of 3D objects has been a topic of significant interest for a large group of researchers for several decades.[1,5–13]

Finite deformation is often involved in the eversion of various structures.[12] The deformation of an everted elastomeric tube has been one of the most classical finite deformation problems since Rivlin[12] first proposed it. Varga[8] has shown that in experiments, except for the regions close to the two ends of the tube, most of the tube after eversion is very close to cylindrical in shape. Chadwick and Haddon have investigated the conditions for the existence and uniqueness of the solutions associated with cylindrical tube eversion.[9] Ericksen[10] and Antman[11] further extended the results to the eversion of spherical shells.

However, an experimental phenomenon associated with tube eversion, first described by Truesdell,[13] has not been well explained for several decades. Truesdell discovered in his experiment that the cross-section of an everted cylindrical tube became noncircular when the tube thickness was large enough. To explain the observation quantitatively, both linear stability analyses[5,6] and weakly nonlinear analyses of tube eversion[7] have been performed by different researchers. These analyses have shown that when the tube thickness is larger than a critical value, the axisymmetric deformation of an everted tube is not stable anymore and wrinkles may appear on the inner surface of the tube after eversion. Nevertheless, as pointed out in many of these articles,[5,6] the critical thickness of the tube predicted by all the previous analyses is significantly larger than the thickness of the tube used in Truesdell's experiment. This well-known discrepancy between the predictions and experiments has not been resolved to date.

In the current study, we fabricate cylindrical elastomer tubes with various sizes using a homemade mold. The material of the tube is a silicone rubber purchased from the company Smooth-On, Inc. (USA). We, for the first time, experimentally demonstrate that when a cylindrical tube is everted as shown in Fig. 1, multiple creases may form on its inner surface, which has been recently identified as a distinct surface instability mode from wrinkles.[14,15] Previous studies have also shown that due to the highly nonlinear deformation associated with crease formation, the critical conditions for crease initiation cannot be predicted using linear or weakly nonlinear analyses.[16] In this article, through energetic analyses and linear perturbation

Department of Mechanical and Aerospace Engineering, University of California, San Diego, La Jolla, CA 92093, USA. E-mail: shqcai@ucsd.edu

† Electronic supplementary information (ESI) available. See DOI: 10.1039/c6sm01381c

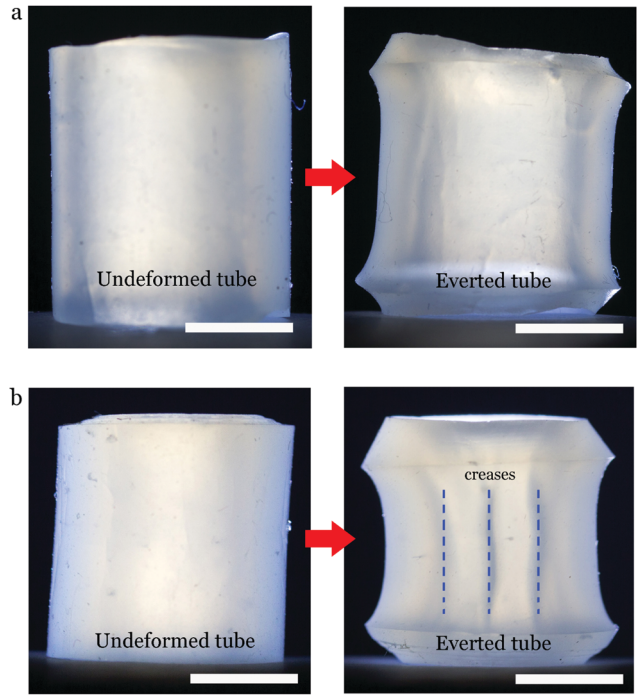

Fig. 1 Crease formation on the inner surface of an everted elastomer tube. (a) If the thickness of the tube is small, after eversion, the inner surface of the tube is smooth and (b) if the thickness of the tube is larger than a critical value, multiple creases form on the inner surface of the everted tube. In the photos above, the outer radius of the tube is 6 mm, while the thickness of the tube in (a) is 2.5 mm and in (b) is 3.0 mm. The length of the scale bar is 5 mm.

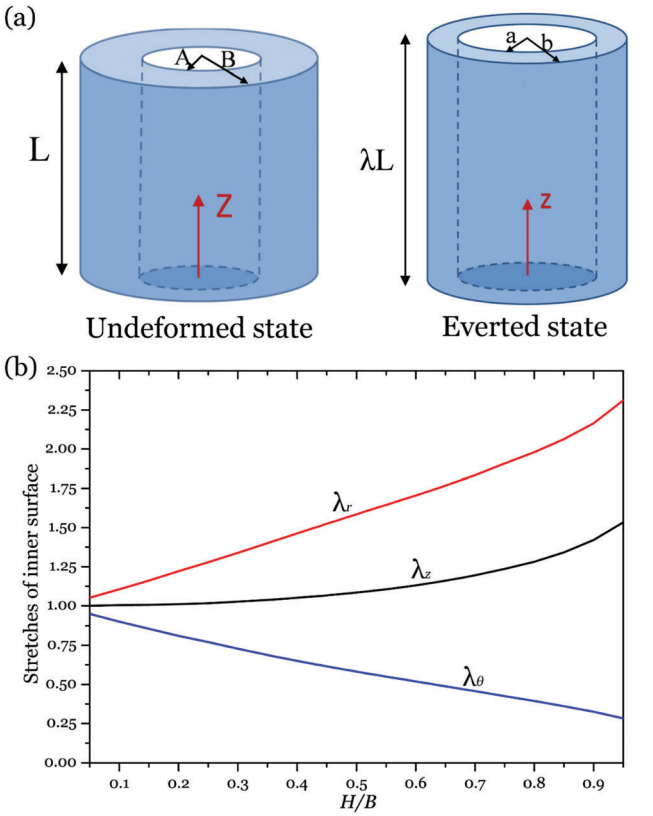

Fig. 2 (a) Schematics of a tube in the undeformed and everted states. (b) After eversion, the stretches in the radial direction λ_r, hoop direction λ_θ and axial directions λ_z of the inner surface of the everted tube are functions of the tube thickness H. In the calculations, we ignore all possible mechanical instabilities.

calculations, we show that creasing instability, instead of wrinkling, should be responsible for the mechanical instability associated with tube eversion.

To study the instability of an everted tube, we first calculate the axisymmetric deformation field of an everted cylindrical tube as shown in Fig. 2a. We use the polar coordinates $X = (R,\Theta,Z)$ to describe the undeformed configuration of the tube and $x = (r,\theta,z)$ for its deformed configuration. As shown in Fig. 2a, the inner and outer radii of the tube in the undeformed state are A and B, and they change to a and b in the everted state. Previous studies have shown that by neglecting the edge effect, the deformation of an everted tube can be simply described by the following fields,[5]

$$r = r(R), \quad \Theta = \theta, \quad z = \lambda Z. \tag{1}$$

The stretch in the radial direction is $\lambda_r = -\mathrm{d}r/\mathrm{d}R$, $\lambda_\theta = r/R$ in the hoop direction, and $\lambda_z = \lambda$ in the axial direction.

With the assumption of axisymmetric deformation, the force balance equation for an everted tube is

$$\frac{\mathrm{d}\sigma_{rr}}{\mathrm{d}r} + \frac{\sigma_{rr} - \sigma_{\theta\theta}}{r} = 0. \tag{2}$$

where σ_{rr} and $\sigma_{\theta\theta}$ are the Cauchy stress in the radial direction and hoop direction, respectively. The boundary condition for the everted tube is $\sigma_{rr} = 0$; on the inner surface: $r = a$, and on the outer surface: $r = b$. Following Rivlin,[12] instead of requiring the normal stress to be zero on the ends of the tube, we relax the boundary conditions to enforce the resultant force applied on the ends of the tube to be zero, namely, $\int_a^b r\sigma_{zz}\mathrm{d}r = 0$. As shown in the early experiments done by Varga,[8] the edge effect in an everted tube only exists for the region around the distance of the thickness of the tube away from its free ends.

For simplicity, we assume that the material of the tube can be described using an incompressible neo-Hookean model.[17] Therefore, we have the following stress–stretch relationship for the material: $\sigma_{rr} = \mu\lambda_r^2 - p$, $\sigma_{\theta\theta} = \mu\lambda_\theta^2 - p$ and $\sigma_{zz} = \mu\lambda_z^2 - p$, where μ is the small-deformation shear modulus of the elastomer and p is hydrostatic pressure. The material is assumed to incompressible, so we have $\lambda_r\lambda_\theta\lambda_z = 1$.

The equilibrium solution of an everted tube can be numerically derived using a shooting method and the details are discussed in Appendix A. Because both the stress boundary conditions and stress balance equations are homogenous, the equations apparently have a trivial solution corresponding to the state without deformation. A nontrivial solution corresponds to the everted state of the tube with finite deformation. In Fig. 2b, we plot the stretches in the radial, hoop and axial directions, λ_r, λ_θ and λ_z, of the inner surface of the everted tube as functions of the normalized thickness of the tube H/B ($H = B - A$). After eversion, the axial and radial stretches are

always larger than one and increases with the thickness of the everted tube. The stretch in the hoop direction decreases as the thickness increases, generating a compressive strain of the inner surface after eversion. A comparison between the experimental measurements and theoretical predictions of the inner and outer radii of the everted tube for a range of thickness H is provided in Fig. S1 (ESI†).

The corresponding stretch and stress fields for a given thickness of $H = 0.5B$ of an everted tube are plotted in Fig. S2 (ESI†). In the radial direction, the stretch λ_r decreases from a value larger than one on the inner surface to a value smaller than one on the outer surface. The radial stress σ_{rr} between the inner and outer surfaces of the tube is always compressive. In the hoop direction, both the stretch λ_θ and stress $\sigma_{\theta\theta}$ are compressive on the inner surface of the everted tube, which may result in surface instability that is shown in Fig. 1b.

As discussed before, wrinkling and creasing are two distinct but commonly observed surface instability modes in soft materials.[14–16] Wrinkles are usually characterized by a smooth undulation while creases are characterized by singular regions of self-contact. Linear perturbation analysis is usually adopted to obtain the critical conditions of wrinkling instability,[18] while a combination of numerical simulation and energetic analyses is used to study crease formation.[15,16] In the following, we calculate the critical conditions for both wrinkling and creasing instabilities of a tube in the everted state.

With the assumption of axisymmetric deformation of an everted tube, we have calculated the deformation field $r = r(R)$ of an everted tube as shown in Appendix A. To conduct linear stability analysis, we perturb the axisymmetric deformation field $r = r(R)$ by a displacement field in both radial direction, $u_r(r,\theta)$, and hoop direction, $u_\theta(r,\theta)$, which further results in perturbations of both the stretch field and stress field. Assuming the perturbations are infinitesimal, we only keep the linear terms of displacement perturbations in the governing equations. Consequently, we obtain an eigenvalue problem, which determines the critical conditions, namely the tube thickness H, for the onset of wrinkles, and the associated eigenvectors describing the modes of wrinkling. A detailed formulation of linear stability analyses can be found in Appendix B. In Fig. S3 (ESI†) we plot the critical tube thickness H for the onset of wrinkles with different wavenumbers. From the calculations, we can conclude that the critical tube thickness for the wrinkling instability associated with eversion is $H_{\text{crit}} = 0.58B$. Similar results have also been reported by Haughton *et al.*[5,6]

Next, we aim at obtaining the critical conditions for creasing instability on the inner surface of an everted tube. As shown in our previous studies,[14] the crease initiation is autonomous, so the critical conditions of creasing can be determined by the local strain field. Based on numerical simulation and energetic analyses, Hong *et al.*[15] obtained the critical conditions for the initiation of a crease on a free surface: $\lambda_1/\lambda_2 = 2.4$, where λ_1 and λ_2 are the two principal stretches on the surface and they correspond to λ_r and λ_θ in cylindrical coordinates adopted in the current tube eversion problem. Comparing the stretch distribution of the inner surface and the critical conditions for crease initiation, as shown in Fig. 2b, we obtain that the critical tube thickness for creasing instability is $H_{\text{crit}} = 0.435B$, which is dramatically smaller than the critical thickness for wrinkling instability predicted based on linear stability analysis. Therefore, creasing is the surface instability mode for an everted tube, which explains why all the previous linear stability analyses overestimated the critical tube thickness. Our statement has also been partially confirmed by the experiment shown in Fig. 1. In Fig. 1a, the inner surface of an everted tube is smooth with the thickness $H = 0.42B$; while in Fig. 1b, creases are visible on the inner surface of the everted tube for the thickness $H = 0.5B$. Although it is not easy to determine the exact thickness for the onset of crease, the critical thickness of the tube has to fall in the range between $0.42B$ and $0.5B$.

We next conduct finite element simulations to further verify the critical conditions for the crease initiation obtained above and to investigate the post-creasing phenomenon of an everted tube. To avoid simulating the complex eversion process, we conduct finite element analysis of the model with initial prestress and prestretch fields as computed from Appendix A. The axial stretch λ_z is kept as a constant in the simulation, so it is a generalized plane strain problem. To simplify the problem, we assume the creases to distribute around the inner surface of an everted tube periodically. Therefore, only a sector of the cross-section of a tube is used in the simulation (inset of Fig. 3). By using the sectors with different angles θ, we can simulate the scenario of an everted tube with different numbers of creases on its inner surfaces. To artificially introduce a crease, we impose a radial displacement at a point on the inner surface of an everted tube as shown in Fig. 3. We then numerically calculate the strain energy of the everted tube as a function of crease depth d. To accurately capture the stress/strain field

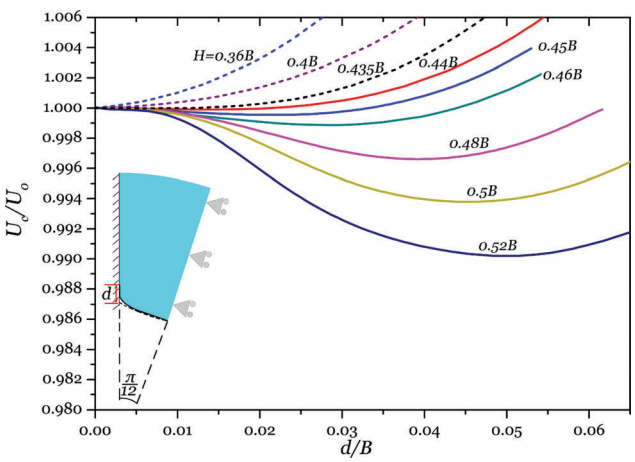

Fig. 3 Normalized strain energy of an everted tube with different thicknesses as a function of crease depth d. When the thickness H is smaller than the critical thickness: $0.435B$ (dash lines), the strain energy of the everted tube increases monotonically with the increase of the crease depth. When the thickness H is larger than the critical thickness (solid lines), the strain energy of the everted tube has a minimum value for a finite crease depth. In the above calculations, we assume that there are 12 creases distributed periodically around the inner surface of the everted tube shown in the inset.

associated with the formation and growth of creases in an everted tube and to improve the convergence of the numerical simulation, we adopt a mesh-to-mesh mapping technique in the simulation (detailed discussion of the simulation procedure can be found in Appendix C). According to our knowledge, the numerical simulation strategy described above has never been reported to model creasing instability in previous studies.

In Fig. 3, we plot the strain energy of the everted tube in the creased state U_c, normalized by the strain energy of the everted tube with an asymmetric smooth deformation U_o, as a function of the normalized crease depth d/B. When the tube thickness H is small, the strain energy of an everted tube increases monotonically with increasing crease depth d. When the tube thickness H is larger than a critical value, namely $0.435B$, the strain energy of the everted tube decreases first with increasing crease depth d, which reaches a minimum for a certain crease depth. Further increase of crease depth will cause an increase of the strain energy. The computational results indicate that when the tube thickness is larger than the critical thickness, the formation of creases on the inner surface of the everted tube can reduce the strain energy. Therefore, the numerical simulation is consistent with our previous predictions of the critical tube thickness for crease formation.

To further predict the total number of creases on the inner surface of an everted tube, by varying the crease depth and the angle of the sector in our simulation, we can compute the minimal strain energy of the everted tube with different numbers of creases. As shown in Fig. 4a, when the thickness of the tube H is larger than the critical thickness, an everted tube with a finite number of creases on its inner surface minimizes the total strain energy. Based on the computational results shown in Fig. 4a, we further plot the number of creases, which minimize the total strain energy of the everted tube, as a function of tube thickness (Fig. 4b). With the increase of tube thickness, the number of creases on the inner surface of everted tubes decreases. Although the normalized energy difference of everted tubes with different numbers of creases is small, the absolute value of the energy difference can be large, compared to the typical thermal fluctuation energy and the energy level associated with most environmental noise. It is reasonable to assume the everted tubes to stay in the configurations with minimal energy, which is also a widely adopted assumption in many previous studies of different mechanical instability patterns.[15,16,19] The predicted result and a microCT (micro-computed tomography) image of a cross-section of an everted tube with a thickness of $H/B = 0.52$ are compared in Fig. 5. It clearly shows that not only the number of creases but also the profile of the inner surface of the everted tube can be well captured by our predictions.

Although our predictions agree well with experimental observations, certain limitations exist in our theory. For example, we assume the distributions of creases are periodic in the inner surface of everted tubes. The assumption may be invalid in certain scenarios. In particular, preexisting defects in the system may predetermine the locations of crease formation.[19] In addition, we adopt the neo-Hookean model to characterize the hyperelasticity

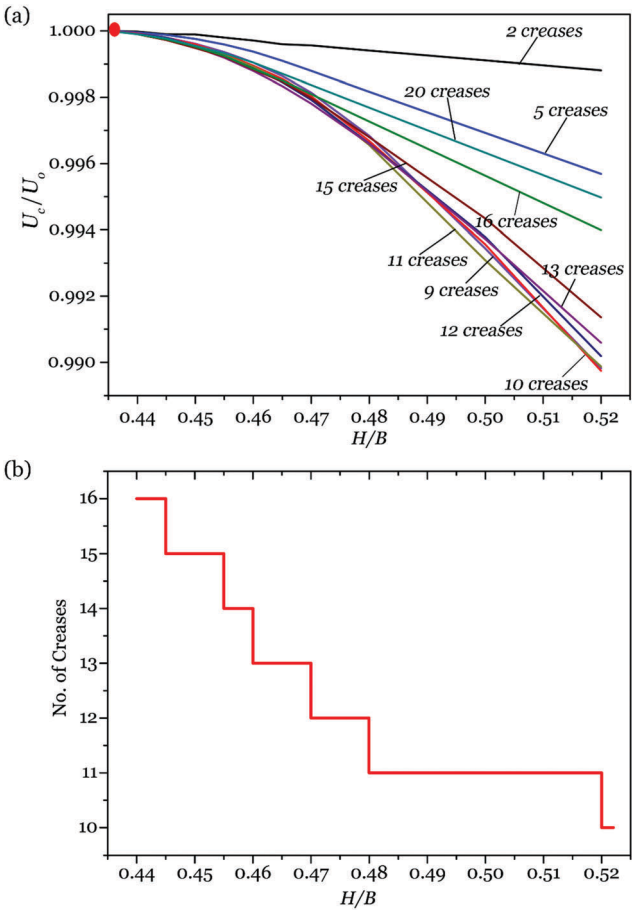

Fig. 4 (a) Normalized strain energy of an everted tube with different numbers of creases. (b) Number of creases on the inner surface of the everted tube with minimal strain energy.

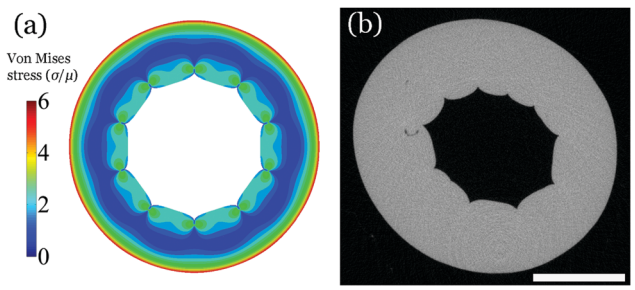

Fig. 5 A comparison between the predicted result (a) and the microCT image (b) of a cross-section of an everted tube with the initial thickness of $H/B = 0.52$. The colors in (a) indicate the von Mises stress normalized by the shear modulus μ of the elastomer. The length of the scale bar is 5 mm.

of elastomers in our experiments, which may be inaccurate for different elastomers. However, as discussed in the reference,[15] the strain involved in the crease formation is finite but modest; the neo-Hookean model should be accurate enough for most elastomers.

In summary, we studied the mechanical instability of an everted cylindrical elastomer tube. By comparing the critical conditions of creasing and wrinkling, we show that the formation

of creases, instead of wrinkles, is the surface instability mode for an everted tube when its thickness is larger than a critical value. Our studies have successfully resolved a long-lasting discrepancy between the theoretical predictions and experimental observations of the critical thickness for an everted tube being unstable. Based on the minimal strain energy assumption, we have also successfully predicted the number of creases formed on the inner surface of a tube after eversion. Our studies of tube-eversion induced creasing in this communication may trigger more investigations of mechanical instabilities associated with eversion of different structures, such as spherical shells.

Acknowledgements

The work was supported by the National Science Foundation through Grant No. CMMI-1538137. We acknowledge Prof. Robert L. Sah of the Department of Bioengineering at UCSD for helping us to take microCT images of an everted tube.

References

1 S. Höhn, A. R. Honerkamp-Smith, P. A. Haas, P. K. Trong and R. E. Goldstein, *Phys. Rev. Lett.*, 2015, **114**, 178101.
2 K. S. Freeman, G. A. Lewbart, W. P. Robarge, C. A. Harms, J. M. Law and M. K. Stoskopf, *Am. J. Vet. Res.*, 2009, **70**, 1087–1093.
3 G. Lewbart, *Invertebrate medicine*, Wiley Online Library, 2006.
4 T. Mizuno, Y. Takewa, H. Sumikura, K. Ohnuma, T. Moriwaki, M. Yamanami, T. Oie, E. Tatsumi, M. Uechi and Y. Nakayama, *J. Biomed. Mater. Res., Part B*, 2014, **102**, 1038–1045.
5 D. Haughton and A. Orr, *Int. J. Non-Linear Mech.*, 1995, **30**, 81–95.
6 D. Haughton and A. Orr, *Int. J. Solids Struct.*, 1997, **34**, 1893–1914.
7 M. S. Pour and Y. Fu, *SIAM J. Appl. Math.*, 2002, **62**, 1856–1871.
8 O. H. Varga, *Stress–strain behavior of elastic materials; selected problems of large deformations*, Interscience, New York, 1966.
9 P. Chadwick and E. Haddon, *IMA J. Appl. Math.*, 1972, **10**, 258–278.
10 J. Ericksen, *Z. Angew. Math. Mech.*, 1955, **35**, 382–385.
11 S. S. Antman, *Arch. Ration. Mech. Anal.*, 1979, **70**, 113–123.
12 R. S. Rivlin, *Philos. Trans. R. Soc. London, Ser. A*, 1949, **242**, 173–195.
13 C. Truesdell, *North-Holland Mathematics Studies*, 1978, vol. 30, pp. 495–603.
14 X. Liang and S. Cai, *Appl. Phys. Lett.*, 2015, **106**, 041907.
15 W. Hong, X. Zhao and Z. Suo, *Appl. Phys. Lett.*, 2009, **95**, 111901.
16 S. Cai, D. Chen, Z. Suo and R. C. Hayward, *Soft Matter*, 2012, **8**, 1301–1304.
17 L. R. G. Treloar, *The physics of rubber elasticity*, Oxford University Press, USA, 1975.
18 M. Biot, *Appl. Sci. Res., Sect. A*, 1963, **12**, 168–182.
19 D. Chen, S. Cai, Z. Suo and R. C. Hayward, *Phys. Rev. Lett.*, 2012, **109**, 038001.

